1,4- vs 1,3-Prototropic Mechanism for Intramolecular Double Proton Transfer Reaction in Monothiooxalic Acid. Theoretical Investigation of Potential Energy Surface

Christophe Raynaud, Jean-Pierre Daudey, Laurent Maron, and Franck Jolibois*

Laboratoire de Physique Quantique, UMR 5626, IRSAMC, Université P. Sabatier, 118 Route Narbonne, 31062 Toulouse, France

Received: May 26, 2005; In Final Form: July 29, 2005

Proton transfer is a very common and important chemical step in many systems. Despite its apparent simplicity, a correct description of this chemical process is difficult from a theoretical point of view. It requires a correct and simultaneous description of a bond breaking and a bond formation. The situation is even much more complicated when two protons are implied. This is the case for monothiooxalic acid, for which two different types (1,3- and 1,4-prototropy) of proton transfers can be invoked. A further problem is the type of the reaction (concerted or not). This paper reports a complete investigation of the potential energy surfaces: characterization of equilibrium points and transitions states. The main conclusion is: the 1,4-prototropic mechanism, mainly considered as a one step concerted exchange of protons, is the most favored from an energetic point of view.

Introduction

Proton-transfer reactions are among the most important mechanisms that can occur in chemistry and biology.[1−6] Despite its apparent simplicity (transfer of a hydrogen atom from one side of a molecular system to another one), this type of reaction has been the subject of a large amount of studies either experimentally or theoretically since many decades. Proton transfer can occur in very different ways. It can proceed through intermolecular or intramolecular reactions, thermal processes on the ground-state potential energy surface, photoinduced transfers involving excited states, etc. Thus, the understanding of such a mechanism remains an exciting challenge. When two protons are transferred during the whole reaction, another question emerges: Does the double proton-transfer process take place in one concerted synchronous mechanism or in a stepwise asynchronous manner?

A theoretical analysis of double proton transfer mechanism using quantum chemical methods mainly consists of investigating parts of the potential energy hypersurface that correspond to the reaction of interest. A better understanding of these potential energy surfaces leads to a better insight into the whole reaction. To improve our knowledge on such chemical process, we decided to study the double proton transfer that may occur in the monothiooxalic acid molecule. This molecular compound may exhibit two double proton transfer mechanisms. One is associated with 1,3-prototropy between geminal heavy atoms (sulfur or oxygen) while the second corresponds to 1,4-prototropy between vicinal heavy atoms. Monothiooxalic acid has recently been the subject of a theoretical work and only one mechanism—1,3-prototropy (see Scheme 1)—has been explored by static quantum chemical approach.[7] The authors managed to characterize four minima and the associated transition states that connect them by pairs. According to their mechanism, double-proton transfer consists of a two-step mechanism. Two different paths can be followed by the molecular system in order to achieve this process. Starting from the absolute minimum (**1**), the first step is either the transfer of proton from S_{A1} to O_{A2} (path 1) that leads to structure **3** or the transfer from O_{B2} to O_{B1} (path 2) that leads to structure **4** (see Scheme 1 for atom numbering and structure definition). The second step is then either the proton transfer from O_{B2} to O_{B1} (path 1) or the transfer from S_{A1} to O_{A2} (path 2) that brings the system to structure **2**. One may note that structure **3** can also connect structure **2** via a rotation process around the carbon−carbon bond with an activation barrier smaller than for a second proton transfer. Rotation can also connect structure **1** and structure **4** and can also be invoked to explain such mechanism. Consequently, rotation around the carbon−carbon bond may correspond either to the first step (transfer via structure **4**) or to the second step of the mechanism (transfer via structure **3**). From a kinetic point of view, the authors of this study have calculated zero-point corrected electronic energy barriers ranging from 27 to 36 kcal·mol^{-1} for proton-transfer reactions and 2.5 kcal·mol^{-1} for rotation around the carbon−carbon bond. From vibrational considerations, it is clear that carbon−carbon bond stretching is a mode that has a high probability to be populated. As a consequence, chemical groups attached to each carbon are coming close together and chemical intuition clearly proposes

SCHEME 1. Reaction Mechanisms for 1,3-Prototropy

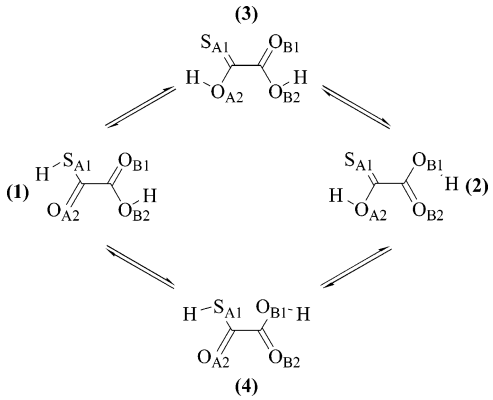

* To whom correspondence should be addressed. E-mail: franck.jolibois@irsamc.ups-tlse.fr.

10.1021/jp052782u CCC: $30.25
Published on Web 10/04/2005

SCHEME 2. Reaction Mechanisms for 1,4-Prototropy

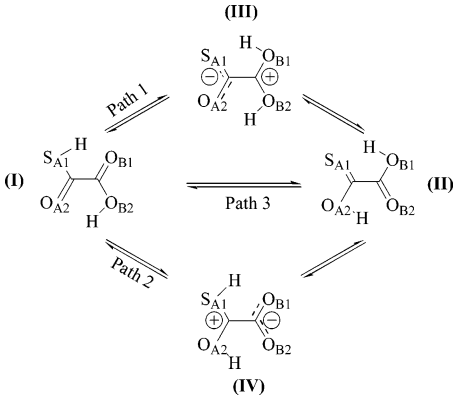

a mechanism for double proton transfer via 1,4-prototropy between vicinal atoms (see Scheme 2). Nevertheless, while 1,4-prototropy seems to be privileged by dynamic considerations, one has first to ensure that it can also be privileged from a static point of view. It must be noted that the preceding study has been performed in a vacuum and did not consider possible modifications of the mechanism if polar solvent is taken into account. Indeed, the proton transfer process might be controlled by the polar environment, and the solvent molecule can be directly involved in the mechanism.[8−10]

The work presented in this article is devoted to the detailed analysis of the potential energy surface (PES) that corresponds to the 1,4-prototropic mechanism of double proton transfer in monothiooxalic acid. Our goal is not only to explain the intrinsic nature of the mechanism but also to show that 1,4-prototropy must be considered to understand double proton transfer in such molecular system. For this purpose, in vacuo static calculations using quantum chemical approaches have been performed in order to describe the energetic and structural aspects of this process and to compare them with Chamorro et al.'s previous work.[7] The principal minima, transition states and one second-order saddle point have been characterized. The PES is described using two reaction coordinates: the $S_{A1}-H$ and $O_{B2}-H$ bond lengths (see Scheme 2 for atom numbering). The main feature of the PES is the existence of only three minima if electronic energy $\Delta_r E$ representation is considered. In the same way, only three transition states (TS) have been fully optimized and characterized. On the other hand, if one uses a Gibbs free energy $\Delta_r G°$ representation of the PES with a 298 K temperature, only two minima and two maxima (TS) can be distinguished, one minimum being higher in energy than a TS. This difference from $\Delta_r E$ representation is mainly explained by the influence of zero point correction term to electronic energies. Ab initio molecular dynamic simulations have then been performed in order to confirm this hypothesis. The classical dynamic investigation clearly indicates that zero point correction terms play an important role in the topology of the Gibbs free energy surface.

By comparing energetic and structural results with those obtained for 1,3-prototropic mechanism, two major conclusions can be reached: (1) the 1,4-prototropic mechanism is energetically favored compared with 1,3-prototropy in the gas-phase and (2) 1,4-prototropy is mainly a quasi-concerted double proton-transfer process with a plateau-type energy profile.

Theoretical Calculations

All static calculations have been performed using the Gaussian 98 suite of programs.[11] Geometry optimizations, frequency calculations and all various potential energy surface scans have been carried out using hybrid DFT functional B3LYP.[12,13] Triple-ζ type basis set augmented by diffuse and polarization functions on all atoms, namely the 6-311++G(d,p) basis set[14] has been used for all calculations. Frequency calculations have been carried out in order to characterize each stationary point (minima, transition state, or second-order saddle point). Finally, intrinsic reaction coordinate calculations[15,16] have been performed to verify that the transition vectors connect, in each case, the corresponding reactant, intermediate or product species. Geometry optimizations were carried out without symmetry constraint. All optimized geometries (Cartesian coordinates) can be obtained as Supporting Information.

Ab initio molecular dynamic (AIMD) simulations have been performed using our own code based on Car−Parrinello type molecular dynamic[17] using atom-centered (Gaussian type orbitals) basis functions.[18] A propagation time step of 0.25 fs was used for each trajectory with the velocity−Verlet integration scheme[19] and a fictitious electronic mass set to 171 au. All dynamic simulations have been performed at a 298.15 K temperature that was controlled by mean of a Nosé−Hoover chain of thermostats.[20,21] First pre-thermalization has been performed at the HF/3-21G(d,p) level during 5 ps using a Born−Oppenheimer approach then thermalization (between 1 and 3 ps) and production (5 ps) dynamic has been done at the B3LYP level. In the last case, core electrons were replaced by an effective core potential with its associated double-ζ basis set[22] augmented with a set of d-polarization functions[23] for carbon, oxygen and sulfur atoms while the 6-311++G(d,p) basis set was used for hydrogen. A thermal Boltzmann distribution was used in order to generate the initial velocities. To estimate free energy variation ($\Delta_r F°$), geometrical constraint dynamic has been performed using "blue moon" ensemble approach.[24] For the first half of path 1 (from **I** to **III**), the projection of the $S_{A1}H$ vector on the $S_{A1}O_{B1}$ vector has been chosen as the constraint while the projection of the $O_{B2}H$ vector on the $O_{B2}O_{A2}$ vector has been employed to describe the second half of this path (from **II** to **III**). In the same way, the same constraints have been employed to describe a part of reaction profile associated with path 2 (from structure **I** to TS_**I_II** and from structure **II** to TS_**I_II**). For each reaction path, the constraint parameter was varied in order to obtain at least 15 constraint values, leading to a total of about 60 trajectories. Finally, for each part of the reaction profile, the free energy variation $\Delta_r F°$ has been calculated according to "blue moon" ensemble theory. One should note that for two reaction profile (first half of path 1 and path 2), the reference ($F° = 0$) is structure **I** while for the two other (second half of each path), the reference was set to structure **II**.

Results and Discussion

Reaction Paths. Because a different basis set has been used compared to that used by Chamorro et al.,[7] characteristic structures of the PES corresponding to the 1,3-prototropic mechanism have been optimized first. With the larger basis set, results are quantitatively identical to those obtained with the other basis set (see Table 1 and ref 7). The potential energy surface can be depicted as follows with two reaction coordinates that mostly describe double proton-transfer reaction path ($S_{A1}-H$ and $O_{B2}-H$ bond lengths): four local minima are connected each other by four transition states with energy barriers $\Delta_r G^{\#}$ ranging from ∼27 to ∼36 kcal·mol^{-1}. Considering the nature of the PES, it clearly appears that the 1,3-prototropic double proton transfer is a two-step process via one path (first transfer

TABLE 1: Electronic (ΔE), Zero-Point-Corrected Electronic ($\Delta_r E_{corr}$) and Gibbs Free ($\Delta_r G$) Energies (in kcal·mol^{-1}), Relative to Structure I, for All Optimized Characteristic Structures Involved in 1,3- or 1,4-Prototropic Double Proton Transfer Reactions[a]

	$\Delta_r E$ (kcal·mol^{-1})	$\Delta_r E_{corr}$ (kcal·mol^{-1})	$\Delta_r G$ (kcal·mol^{-1})
I	0.0	0.0	0.0
TS_**I_III**	17.2	16.4	16.9
III	16.9	17.9	18.2
TS_**III_II**	18.5	18.1	18.7
II	2.5	4.5	4.8
TS_**I_II**	22.9	21.5	22.1
saddle_**I_II**	25.6	21.9	22.7
1	2.3	2.1	1.7
TS_**1_3**	37.9	35.9	34.9
3	6.7	8.6	7.7
TS_**3_2**	44.6	43.4	42.3
2	6.7	8.6	7.8
TS_**2_4**	37.9	35.9	34.9
4	3.6	3.3	2.5
TS_**1_4**	42.0	38.8	38.0

[a] Electronic energies correspond to geometries that have been optimized at the B3LYP/6311++G(d,p) theoretical level and Gibbs free energies come from frequencies calculations analysis at 298 K using the same theoretical level.

from S_{A1}−H group) or the other one (first transfer from O_{B2}−H group).[7] Tunneling effects are relevant when one considers proton-transfer reactions[25] and can have significant impact on reaction rate constants. A rough estimate of tunneling effect can be provided by the Wigner expression which gives a temperature dependent transmission coefficient in terms of the single imaginary frequency of the transition structure.[26] Such coefficients estimated using imaginary frequencies calculated by Chamorro et al.[7] lie between 4 and 5. However, if one considers the plateau-type potential energy profile associated with the 1,4-prototropic mechanism (see below for details), this quantum effect can be neglected.[27,28] Indeed, the height and the shape of the potential mainly determine tunneling effect. However, the barrier of the proton-transfer reaction is broad because it adopts a plateau type energy profile (see below) and thus this feature will lower the transmission coefficient. Consequently, tunneling effect has not been taken into account for the double proton-transfer reactions.

It appears from our calculations that all geometries involved in 1,4-prototropic mechanism (minima, transition states, and second-order saddle point) exhibit a planar conformation that is essentially due to hydrogen-bond type intramolecular interactions involving S_{A1},O_{B1}, and H atoms on one side and O_{A2}, O_{B2}, and H atoms on the other side. Consequently, rotation around the C−C bond might involve larger energy barriers that come from breaking intramolecular interactions and will not be invoked for double-proton-transfer mechanism.

Among all geometries optimized from compounds **1**−**4** and **I**−**IV** (see Schemes 1 and 2 for structure notation), the global electronic energy minimum corresponds to structure **I**, which is lower in energy compared to all the other minima as presented in Table 1. For the 1,4-prototropic mechanism, the reaction that goes from the global minimum (**I**) to the final product (**II**) can involve three different energy paths. The first one (path 1) corresponds to a double proton transfer that starts with the transfer of the hydrogen attached to the S_{A1} sulfur atom and the second one (path 2) to a similar mechanism that is initiated by the transfer of the hydrogen attached to the O_{B2} oxygen. The third mechanism (path 3) is associated with concerted transfer of both hydrogen atoms. Consequently, one expects to find transition states in the first two mechanisms while a second-order saddle point is anticipated for the last one.

Along this first reaction path (path 1 in Figure 1 and Scheme 2), a stable zwitterionic intermediate (**III**) has been fully optimized and is located 16.9 kcal·mol^{-1} higher in electronic energy compared to the reactant (**I**) energy (see Figure 1 and $\Delta_r E$ value in Table 1). The complete proton transfer from sulfur atom S_{A1} toward the oxygen atom O_{B1} characterizes this local minimum. It connects with the reactant (**I**) through a transition state (TS_**I_III**) with an electronic energy barrier of 17.2 kcal·mol^{-1} with respect to the global minimum. Consequently, the reverse reaction (from **III** to **I**) requires only 0.3 kcal·mol^{-1} to be achieved. Frequencies calculation on this transition state indicates an imaginary frequency (593*i* cm^{-1}) characterized by a transition vector that involved the motion of hydrogen atom from S_{A1} to O_{B1} (Figure 2a). Following this path, product **II** is predicted to be 2.5 kcal·mol^{-1} less stable than **I**. This product is reached through another transition state (TS_**III_II**) located 18.5 kcal·mol^{-1} above the global minimum (**I**). Thus, the necessary electronic energy barrier for the path from **III** to **II** is less than 2 kcal·mol^{-1}. The transition vector (imaginary frequency = 868*i* cm^{-1}, see Figure 2b) corresponds to the motion of the second hydrogen from oxygen O_{B2} to oxygen O_{A2}, thus completing the whole reaction. One should note that TS_**I_III**, **III**, and TS_**III_II** are extremely close in energy (within 2 kcal·mol^{-1}).

Concerning the second reaction path (path 2 in Figure 1 and Scheme 2), among all hypothetic molecular structures, several attempts to optimize the intermediate (**IV**) have failed. Instead, only one transition state, (namely TS_**I_II**), has been localized in this region of the PES at ∼23 kcal·mol^{-1} (see Table 1 and Figure 1). Intrinsic reaction coordinate calculation starting from this transition state clearly indicates that it connects reactant **I** to product **II**. The transition vector (imaginary frequency = 440*i* cm^{-1}) represented in Figure 2c exhibits one major component corresponding to the proton transfer from S_{A1} to O_{B1} and a minor one related to proton transfer from O_{B2} to O_{A2}. Moreover, the O_{B2}−H bond length has considerably increased (bond length variation from global minimum geometry of 0.8 Å) and the O_{A2}−H bond is almost created (bond length = 1.013 Å compared with equilibrium distance for minimum **II** of 0.98 Å). The existence of such transition state and the characteristic of its transition vector clearly indicates that the second path (Path 2 in Figure 1and Scheme 2)—first transfer of the proton attached to the oxygen atom O_{B2} followed by transfer of the hydrogen atom connected to S_{A1}- is a quasi-concerted one step double proton transfer characterized by a "plateau" type energy profile. This double proton transfer mechanism can be depicted as a superposition of two single proton transfers that are characterized by an extended overlap of the associated potentials. Consequently, the zwitterionic intermediate (**IV**) that was expected between the two transition states is destabilized and the first transition state from structure **I** to **IV** cannot be obtained. Therefore, the transition structure that has been optimized (TS_**I_II**) corresponds mainly to the transition state between the hypothetic zwitterionic structure **IV** and the final product (**II**). The associated transition vector that essentially describes the second proton-transfer process confirms the hypothesis.

Finally, a second-order saddle point, saddle_**I_II**, has been optimized and well characterized by two imaginary frequencies that correspond on one hand to an antisymmetric stretching mode (1517*i* cm^{-1}) and on the other hand to a symmetric one (856*i* cm^{-1}) as represented in Figure 3a and 3b, respectively. This second-order saddle point was found 25.6 kcal·mol^{-1} higher in energy than **I** (see Table 1 and Figure 1) and is associated with the third reaction path. However, this peculiar

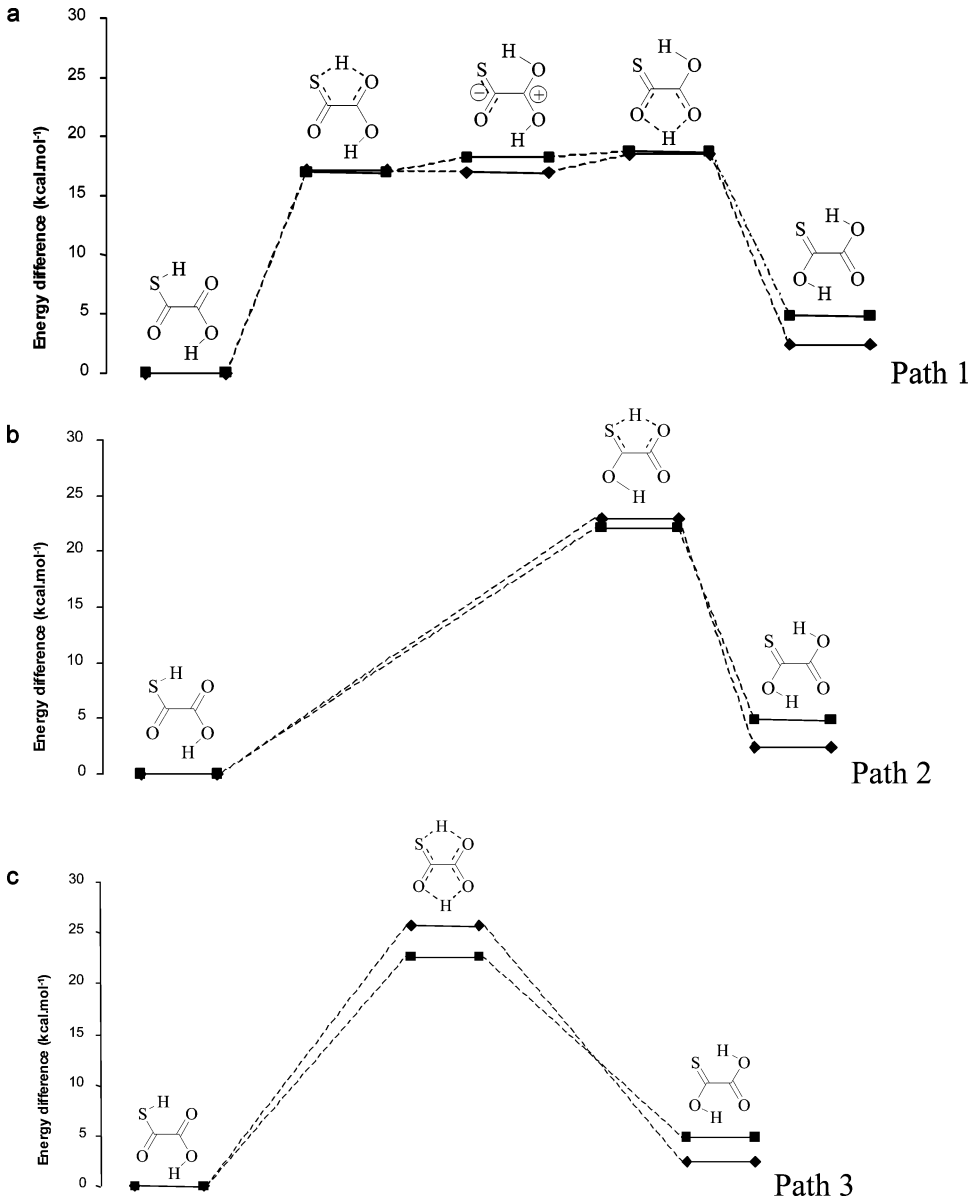

Figure 1. B3LYP/6-311++G(d,p) relative electronic energies (diamonds) and relative Gibbs free energies at $T = 298.15$ K (squares) corresponding to 1,4-prototropic double proton-transfer process. Path 1 implies a first transfer from $H-S_{A1}$ hydrogen followed by $H-O_{B2}$ transfer. Path 2 involves a first transfer from $H-O_{B2}$ hydrogen followed by $H-S_{A1}$ transfer. Path 3 corresponds to the concerted double proton transfer via a second-order saddle point.

region of the PES remains close in energy to the previously described reaction path.

Free Energy Analysis. Electronic energy representation of the PES directly comes from optimized geometries calculations. However, the effectiveness of a chemical reaction arises from its Gibbs free energy analysis. Such analysis has been performed at the standard 298 K temperature directly from frequencies calculations. Results are reported in Table 1 and Figure 1. For path 3, a 3 kcal·mol^{-1} decrease of the energy barrier is observed while the barrier for reaction path 2 is reduced by only 0.8 kcal·mol^{-1}. The main difference compared with the previous electronic energy representation (see above) essentially concerns the first reaction path. When one considers calculated Gibbs free energies, intermediate structure **III** that was 0.3 kcal·mol^{-1} more stable than transition state TS**_I_III** is now 1.3 kcal·mol^{-1} less stable (see Table 1 and Figure 1). Moreover, while the electronic energy barrier necessary to perform the **III** to **II** mechanism is almost equal to 2 kcal·mol^{-1}, the corresponding Gibbs free energy barrier is only 0.5 kcal·mol^{-1}. Detailed examination of all contributions to the Gibbs free energy shows that the main energy modifications are due to zero-point energy corrections. Calculation of zero-point corrected electronic energies (ΔE_{corr}) reveals a stabilization of TS**_I_III** by 0.8 kcal·mol^{-1} while the intermediate **III** is destabilized by almost 1 kcal·mol^{-1} compared to electronic energies. This zero-point energy contribution to transition state stabilization has already been observed in the theoretical investigation of oxalic acid.[29] While the overlap of the two electronic energy potential associated with single proton transfer is small enough to allow the existence of the intermediate (**III**), this overlap is larger if one considers Gibbs free energy potentials thus leading to the destabilization of this zwitterionic structure. These results must be taken with extreme care if one keeps in mind that the potential energy surface in the vicinity of the intermediate region is extremely flat. As a consequence, harmonic approximations used to calculate thermal corrections (entropic terms, etc.) and some quantum nuclear effects (zero-point energy) may be questionable in this case and thus might leads to suspicious energy values.

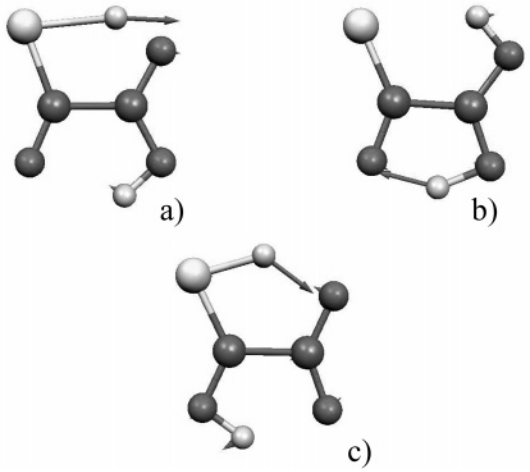

Figure 2. Transition state structures and transition vectors of (a) TS_**I_III** (imaginary frequency = 593*i* cm^{-1}), (b) TS_**III_II** (imaginary frequency = 868*i* cm^{-1}) and (c) TS_**I_II** (imaginary frequency = 440*i* cm^{-1}). Results come from frequencies calculations performed at the B3LYP/6-311++g(d,p) theoretical level.

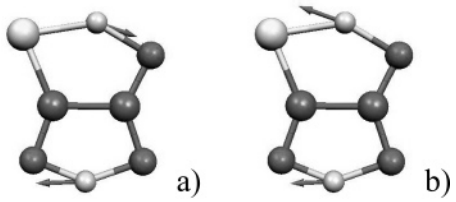

Figure 3. Second-order saddle point saddle_**I_II** structure and transition vectors. a) antisymmetric vibrational mode (imaginary frequency = 1517*i* cm^{-1}); (b) symmetric vibrational mode. (imaginary frequency = 856*i* cm^{-1}). Results come from frequency calculations performed at the B3LYP/6-311++g(d,p) theoretical level.

For instance, a constrained ab initio molecular dynamic might be a good alternative to extract more accurate values. This type of molecular dynamic that is based on classical description of nuclear motion does not take into account quantum effects such as zero point energy. However, such dynamic can describe more accurately the free energy profile by including directly all thermal effects beyond the harmonic approximation. Free energy profiles extracted from our dynamic calculations are presented in Figure 4. Concerning reaction path 1 (Figure 4a), each dynamic analysis succeeds in revealing the existence of a zwitterionic intermediate and the activation barriers are close to those obtain by static calculations. The difference between static and dynamic results can be explained by the fact that pseudo-potentials were used for dynamic study while all electron calculations were performed for the static approach. This result indicates that the harmonic approximation might not be invoked to explain the destabilization of the zwitterionic intermediate when one goes from electronic energy description to Gibbs free energy representation. As a consequence, one must include the zero point energy correction to our dynamic scheme in order to confirm the influence of such contribution to the whole energy profile. Such correction and more generally quantum nuclear effect corrections can be included using mixed quantum-classical dynamics associated with path integrals method.[30,31] Moreover, adiabatic switching approach[32,33] can be used to estimate anharmonic zero point energy correction, and its implementation in our own dynamic code is currently under development. For reaction path 2 (Figure 4b), a "plateau" type profile has been obtained with free energy value in agreement with static calculations. One should note that dynamics around the transition state (TS_**I_II**) have led to the transfer of the second proton and consequently we did not manage to extract free energy value in this region of the surface. To resolve this problem, it might be necessary to perform dynamics with two constraints associated with the double proton-transfer mechanism and this work is under investigation.

These results show that the "plateau" type profile associated with double proton transfer reaction emerges not only from uncorrected potential energy surfaces as obtained for reaction path 2 but also from the more physically significant zero point corrected one that has been determined for path 1. This peculiar feature has recently been theoretically observed and discussed in the case of double proton transfer between substituted pyrazoles and guanidine system.[34]

Mechanistic Description. Going back to the results obtained by static approach, the topology of the PES either using electronic energy or Gibbs free energy indicates that the reaction profile almost adopts a "plateau" type transition region[27,28] as observed for reaction path 2. One may note that Gibbs free energy barriers associated with path 2 and path 3 are very close together (energy difference of 0.6 kcal·mol^{-1}). Moreover, these barriers are 3.4 and 4.0 kcal·mol^{-1} higher, for path 2 and path 3 respectively, than those obtains for the first mechanism. As a consequence, neither of these reaction paths via TS_**I_II** or saddle_**I_II** can be privileged. Moreover the hypothesis of a one step double proton-transfer reaction path is now confirmed by this result that indicates that no stable intermediate exists between stationary points **I** and **II** if Gibbs free energies in the gas phase is considered. To obtain further insight into the mechanism associated with the double proton-transfer processes, structural modifications along reaction paths have been analyzed. Structural behaviors have been put in evidence by studying the evolution of several geometric parameters. These features have been extracted from the intrinsic reaction coordinate calculations that have been performed starting from each transition state (Figure 5). In particular, the evolution of the distance between chemical groups attached to each carbon allows the understanding of how proton transfers proceed during the reaction. For path 1 and path 2, the double proton-transfer proceeds in four steps. The first step corresponds to a reduction (0.3 Å) of the distance between two heavy atoms from one side of the molecule (S_{A1}, O_{B1} for path 1, O_{A2}, O_{B2} for path 2) compared to the reactant structure (see Figure 5, parts a and c). Then, a first proton transfer occurs between the two heavy atoms that is characterized by the increase of the $S_{A1}-H$ (path 1, Figure 5c) or $O_{B2}-H$ (path 2, Figure 5a) bond length. This transfer is also linked to an increase of the distance between the two previously cited heavy atoms at the end of the process. The third step involves a diminution (0.3 Å) of the distance between the two heavy atoms from the other side of the molecule (O_{A2}, O_{B2} for path 1, S_{A1}, O_{B1} for path 2) compared to the reactant structure (see Figure 5, parts d and b); Finally, the second proton transfer between the two heavy atoms happens (increase of the $O_{B2}-H$ for path 1 or $S_{A1}-H$ for path 2 bond length). As previously, this last process is connected to an increase of the distance between the two previously cited heavy atoms. As a consequence, proton-transfer processes are connected to a first displacement of the heavy atoms between which the hydrogen migrates. These results are similar to the ones that have been obtained for double proton transfer in oxalamidine for which the two nitrogen are brought together before proton migrates from one side of the molecule to the other.[35] Moreover, the importance of heavy atoms motion has also been carefully

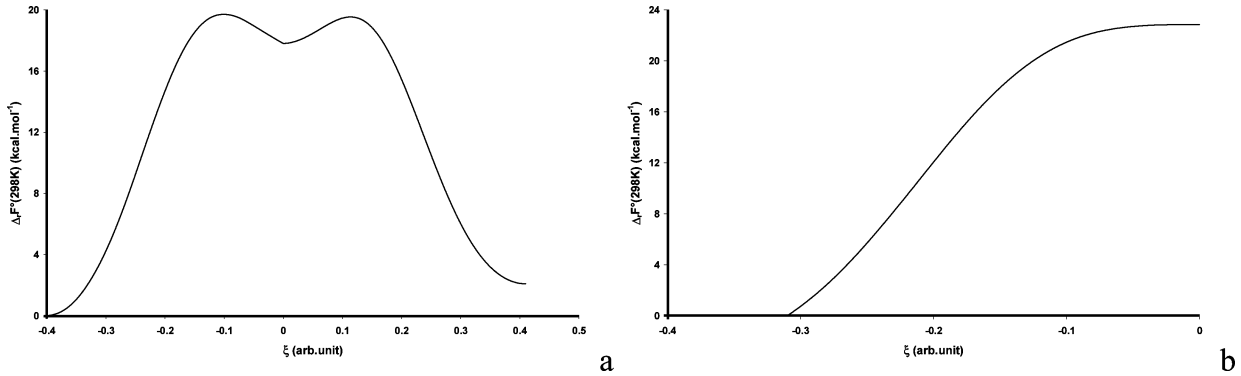

Figure 4. Reaction energy profile extracted from constraint ab initio molecular dynamics: (a) energy profile for path 1; (b) energy profile for path 2.

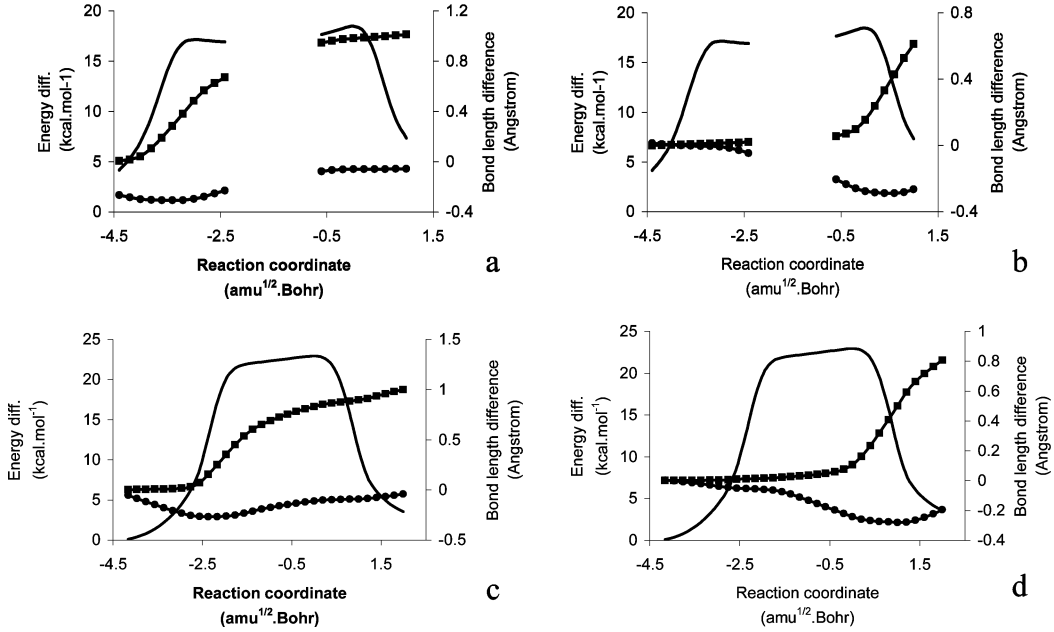

Figure 5. Energy profile and selected bond lengths variation along the intrinsic reaction path evaluated at the B3LYP/6-311++G(d,p) level. (a) $S_{A1}-O_{B1}$ and $S_{A1}-H$ bond length variation along the reaction path 1; (b) $O_{A2}-O_{B2}$ and $O_{B2}-H$ bond length variation along the reaction path 1; (c) $O_{A2}-O_{B2}$ and $O_{B2}-H$ bond length variation along the reaction path 2; (d) $S_{A1}-O_{B1}$ and $S_{A1}-H$ bond length variation along the reaction path 2. Parts a and b are each the combination of two intrinsic reaction path calculations, and the gap between −2.5 and −0.5 has no physical significance but is just introduced for clarity.

described for double proton transfer in benzoic acid dimer using combined experimental and theoretical analysis.[36−38]

1,3- vs 1,4-Prototropy. Let us consider now the two possible ways to undergo double proton transfer in monothiooxalic acid, either 1,3- or 1,4-prototropy. 1,3-prototropy Gibbs free potential energy surface is characterized by four local minima that are connected together by transition states located between 33 and 40 kcal·mol^{-1} from structure **1**. On the other hand, 1,4-prototropy mechanism mainly occurs in a double-well like potential energy surface with first and second-order saddle points ranging from 19 to 23 kcal·mol^{-1} from structure **I**. As a consequence, the last mechanism is energetically more favorable than 1,3-prototropy in the gas phase. Moreover, the efficiency of double proton transfer can be interpreted in term of reaction path. On one hand, one observes that 1,3-prototropy is a two-step nonconcerted double proton transfer. On the other, the mechanism involves during 1,4-prototropy is clearly a one step quasi-concerted process. Thus, when one proton is transferred during 1,3-prototropy the probability to achieve the second proton transfer may not be equal to one. One can observe back transfer to the initial structure or the molecule can be trapped in an intermediate state. If one proton is transferred, the second will be automatically displaced to the other side of the molecule according to the reaction paths proposed for 1,4-prototropy.

Conclusion

In this paper, we propose another mechanism for intramolecular double proton transfer that can occur in monothiooxalic acid in the gas phase. Potential energy surface for 1,4-prototropy has been investigated by the way of static and dynamic theoretical hybrid DFT calculations. The principal regions of the potential energy surface have been fully characterized according to our computational scheme. Our results give evidence that 1,4-prototropic mechanism is favorable on an energetic point of view compared to 1,3-prototropy. We found activation barriers that are 20 kcal·mol^{-1} lower than in the case of 1,3-prototropy. While one zwitterionic intermediates has been localized for one electronic energy path, among the two possible, a Gibbs free energy representation exhibits two reaction mechanism characterized by a plateau type energy profile. These results suggest that no stable intermediate exists between the regions of reactant and product compounds in the gas phase. Ab initio molecular dynamic simulations have demonstrated that if zero point energy corrections are not taken into account the

zwitterionic intermediate is not destabilized compared to electronic energy profile. Thus, such quantum effect must be included in the dynamic approach in order to correctly describe the reaction process. Thus, 1,4-prototropy is a quasi-concerted double proton transfer that mainly occurs in one step. However, one may consider that such zwitterionic intermediate will be stabilized if a polar solvent is considered.[28] In the same way, the whole reaction profiles, either for 1,3- or 1,4-prototropy, might be modified and the stepwise mechanism would probably be favored if polar solvent effects are considered. Consequently, the complete analysis of these mechanisms needs a new investigation in such conditions.

To obtain further insight into the intrinsic nature of the 1,4-prototropic mechanism, one may invoke the characteristics of the heavy atoms present in monothiooxalic acid (sulfur and oxygen, for instance). However, the study of this system alone is not sufficient to clearly answer this issue and further analysis of 1,4-prototropy on similar molecules such as oxalic, dithiooxalic, trithiooxalic, and quadrithiooxalic acid must be considered.

Acknowledgment. This work is supported by a grant from the French Ministry of Research (ACI 'jeunes chercheurs" No. 4009).

Supporting Information Available: Tables giving Cartesian coordinates of all optimized characteristic structures on the potential energy surface associated with the 1,4-prototropic mechanism. This material is available free of charge via the Internet at http://pubs.acs.org.

References and Notes

(1) Bell, R. P. *The proton in chemistry*; Cornell University Press: Ithaca, NY, 1959.
(2) Borgis, D.; Hynes, J. T. The enzyme catalysis process. In *NATO ASI Series A: Life sciences*; Cooper, A., Houben, J., Chien, L., Eds.; Plenum Press: New York, 1989; Vol. 178; p 293−303.
(3) Brzezinski, P. *Biochim. Biophys. Acta* **2000**, *1458*, 1−5.
(4) Devault, D. *Quantum mechanical tunneling in biological systems*; Cambridge University Press: London, 1984.
(5) Krishtalik, L. I. *Biochim. Biophys. Acta* **2000**, *1458*, 6−27.
(6) Szafran, M. *J. Mol. Struct.* **1996**, *381*, 39−64.
(7) Chamorro, E.; Toro-Labbe, A.; Fuentealba, P. *J. Phys. Chem. A* **2002**, *106*, 3891−3898.
(8) Ando, K.; Hynes, J. T. *J. Phys. Chem. B* **1997**, *101*, 10464−10478.
(9) Gertner, B. J.; Peslherbe, G. H.; Hynes, J. T. *Isr. J. Chem.* **1999**, *39*, 273−281.
(10) Al-Halabi, A.; Bianco, R.; Hynes, J. T. *J. Phys. Chem. A* **2002**, *106*, 7639−7645.
(11) Frisch, M. J.; Trucks, G. W.; Schlegel, H. B.; Scuseria, G. E.; Robb, M. A.; Cheeseman, J. R.; Zakrzewski, V. G.; Montgomery, J. A.; Stratmann, R. E., Jr.; Burant, J. C.; Dapprich, S.; Millam, J. M.; Daniels, A. D.; Kudin, K. N.; Strain, M. C.; Farkas, O.; Tomasi, J.; Barone, V.; Cossi, M.; Cammi, R.; Mennucci, B.; Pomelli, C.; Adamo, C.; Clifford, S.; Ochterski, J.; Petersson, G. A.; Ayala, P. Y.; Cui, Q.; Morokuma, K.; Malick, D. K.; Rabuck, A. D.; K.; R.; Foresman, J. B.; Ortiz, J. V.; Cioslowski, J.; Stefanov, B. B.; Liu, G.; Liashenko, A.; Piskorz, P.; Komaromi, I.; Gomperts, R.; Martin, R. L.; Fox, D. J.; Keith, T.; Al-Laham, M. A.; Peng, C. Y.; Nanayakkara, A.; Gonzalez, C.; Challacombe, M.; Gill, P. M. W.; Johnson, B.; Chen, W.; Wong, M. W.; Andres, J. L.; Gonzalez, C.; Head-Gordon, M.; Replogle, E. S.; Pople, J. A. Revision A.9 ed.; Gaussian Inc.: Pittsburgh, PA, 1998.
(12) Becke, A. D. J. *J. Chem. Phys.* **1993**, *98*, 5648−5652.
(13) Lee, C.; Yang, W.; Parr, R. G. *Phys. Rev.* **1988**, *B37*, 785−789.
(14) Description of basis sets can be found in the following: Foresman, J. B. F.; A. Frisch. In *Exploring chemistry with electronic structure methods*, 2nd ed.; Gaussian Inc.: Pittsburgh, PA 1998.
(15) Fukui, K. *Acc. Chem. Res.* **1981**, *14*, 363−368.
(16) Gonzalez, C.; Schlegel, H. B. *J. Phys. Chem.* **1990**, *94*, 5523−5527.
(17) Car, R.; Parrinello, M. *Phys. Rev. Lett.* **1985**, *55*, 2471.
(18) Raynaud, C.; Maron, L.; Daudey, J.-P.; Jolibois, F. *Phys. Chem. Chem. Phys.* **2004**, *6*, 4226.
(19) Verlet, L. *Phys. Rev.* **1967**, *159*, 98.
(20) Hoover, W. G. *Phys. Rev. A* **1985**, *31*, 1695.
(21) Nosé, S. *J. Chem. Phys.* **1984**, *81*, 511.
(22) Bergner, A.; Dolg, M.; Kuechle, W.; Stoll, H.; Preub, H. *J. Mol. Phys.* **1993**, *80*, 1431.
(23) Maron, L.; Teichtel, C. *Chem. Phys.* **1998**, *237*, 105.
(24) Sprik, M.; Ciccotti, G. *J. Chem. Phys.* **1998**, *109*, 7737.
(25) Loerting, T.; Liedl, K. R. *J. Am. Chem. Soc.* **1998**, *120*, 12595−12600.
(26) Steinfeld, J. E.; Francisco, J. S.; Hase, W. L. In *Chemical kinetics and dynamics*; Prentice Hall: Englewood Cliffs, NJ, 1999.
(27) Rauhut, G. *Phys. Chem. Chem. Phys.* **2003**, *5*, 791−800.
(28) Schweiger, S.; Rauhut, G. *J. Phys. Chem. A* **2003**, *107*, 9668−9678.
(29) Higgins, J.; Zhou, X.; Liu, R.; Huang, T. T.-S. *J. Phys. Chem. A* **1997**, *101*, 2702−2708.
(30) Marx, D.; Parrinello, M. *J. Chem. Phys.* **1996**, *104*, 4077−4082.
(31) Hammes-Schiffer, S. *Curr. Opin. Struct. Biol.* **2004**, *14*, 192−201.
(32) Solov'ev, E. A. *Sov. Phys. JETP* **1978**, *48*, 635.
(33) Skodje, R. T.; Borondo, F.; Reinhardt, W. P. *J. Chem. Phys.* **1985**, *82*, 4611−4632.
(34) Schweiger, S.; Hartke, B.; Rauhut, G. *Phys. Chem. Chem. Phys.* **2005**, *7*, 493−500.
(35) Kim, Y.; Hwang, H. J. *J. Am. Chem. Soc.* **1999**, *121*, 4669−4676.
(36) Meyer, R.; Ernst, R. R. *J. Chem. Phys.* **1987**, *86*, 784−801.
(37) Meyer, R.; Ernst, R. R. *J. Chem. Phys.* **1990**, *93*, 5518−5532.
(38) Stöckli, A.; Meier, B. H.; Kreis, R.; Meyer, R.; Ernst, R. R. *J. Chem. Phys.* **1990**, *93*, 1502−1520.